Constraining new physics with searches for long-lived particles: Implementation into SModelS

Jan Heisig[a], Sabine Kraml[b], Andre Lessa[c]

[a] *Institute for Theoretical Particle Physics and Cosmology, RWTH Aachen University, 52056 Aachen, Germany*
[b] *Laboratoire de Physique Subatomique et de Cosmologie, Université Grenoble-Alpes, CNRS/IN2P3, 53 Avenue des Martyrs, F-38026 Grenoble, France*
[c] *Centro de Ciências Naturais e Humanas, Universidade Federal do ABC, Santo André, 09210-580 SP, Brazil*

Abstract

We present an implementation of heavy stable charge particle (HSCP) and R-hadron signatures into SModelS 1.2. We include searches performed at the 8 and 13 TeV LHC and show the capabilities by applying SModelS 1.2 to two new physics scenarios: the inert doublet model and a gravitino dark matter scenario. In the former we find sensitivity up to dark matter masses of 580 GeV for small mass splitting within the inert doublet while missing energy searches are not able to constrain any significant part of the cosmologically allowed parameter space of the model. The gravitino dark matter scenario provides a larger variety of simplified model topologies. We show that both HSCP and R-hadron searches provide important constraints potentially allowing us to conclude on the valuable range of the reheating temperature.

1. Introduction

Exploring physics beyond the standard model (BSM) is one of the key scientific goals of the LHC. Simplified models have turned out to provide useful benchmarks for interpreting LHC results and investigating their implications aiming to answer the open questions of today's fundamental physics. SModelS [1, 2] provides a very efficient framework for this reinterpretation by decomposing the signal of an arbitrary new physics model (respecting a $\mathcal{Z}_2$ symmetry or a larger symmetry with a $\mathcal{Z}_2$ subgroup) into simplified model topologies. This allows one to directly use the cross-section upper limits or efficiency maps provided by the experimental collaborations within the simplified model framework to constrain a larger variety of BSM scenarios.[1]

So far SModelS assumed that all stable particles were neutral and only included BSM searches for missing transverse momentum (MET). However, it has widely been recognized that well-motivated BSM theories can provide non-neutral long-lived particles (LLPs) leading to distinct signatures, often providing great sensitivity at the LHC []. In this letter we make use of the novel features of SModelS 1.2 [7] to investigate well-motivated full BSM models containing LLPs. Besides being able to decompose models with long-lived charged particles, this version also includes a treatment of metastable particles and constraints for heavy stable charged particles (HSCPs) and R-hadrons[2] in its database. In particular, we improve upon previous work [8] adding efficiency maps for the CMS 13 TeV HSCP analysis [9] and reconsidering the modeling of intermediate lifetimes. We also include the experimental cross-section upper limits for the direct production of HSCPs [9, 10] and R-hadrons [9]. Finally, SModelS 1.2 is made publicly available.[3]

We make use of SModelS 1.2 to investigate how the searches for HSCPs and R-hadrons mentioned above impact two new physics scenarios. The first one, the Two Higgs Inert Doublet Model (IDM), provides one of the simplest dark matter models supplementing the Standard Model by just one additional $SU(2)$ (Higgs) doublet. While MET searches are scarcely sensitive to the cosmologically allowed region of the IDM parameter space, we show that for small mass splittings within the inert doublet a large range of dark mat-

[1] A certain degree of approximation is included in this procedure, since it neglects properties like the exact production mechanism and the spin of the particles in decays, see Ref. [3–6] for specific discussions.

[2] For simplicity we label electrically charged and color neutral heavy stable particles as HSCPs. Long-lived colored particles, which can hadronize and form electrically charged bound states are always referred to as R-hadrons.

[3] The SModelS tool and database are available at http://smodels.hephy.at

ter masses can be tested by the HSCP searches.

Secondly, we consider the minimal supersymmetric standard model (MSSM) where the gravitino is assumed to be the lightest supersymmetric particle (LSP) and the stau to be next-to-LSP (NLSP). This is a cosmologically attractive scenario allowing to alleviate the gravitino problem [11–14] and to accommodate large reheating temperatures $T_{\mathrm{R}} \sim 10^9$ GeV in the early Universe while respecting bounds from big bang nucleosynthesis (BBN) []. The complexity of the model reveals a large number of contributing topologies including R-hadron signatures relevant for both squarks and gluinos when their decays are 3- or 4-body suppressed. We show that the LLP results have the potential to be competitive with cosmological constraints and impact the allowed range for the reheating temperature. *[Some more refs?]*

The remainder of this letter is structured as follows. In Sec. 2 we briefly review the implementation of LLP signatures into SModelS. The impact for the IDM and gravitino scenarios is presented in Sec. 3. We conclude in Sec. 4. Finally, in Appendix A and Appendix B we provide details about the recasting of the HSCP analyses and a discussion about the treatment of intermediate lifetimes, respectively.

2. Implementation in SModelS

Exploring physics beyond the standard model (BSM) is one of the key scientific goals of the LHC. Simplified models have turned out to provide useful benchmarks for interpreting LHC results and investigating their implications aiming to answer the open questions of today's fundamental physics. SModelS [1, 2] provides a very efficient framework for this reinterpretation by decomposing the signal of an arbitrary new physics model (respecting a $\mathcal{Z}_2$ symmetry or a larger symmetry with a $\mathcal{Z}_2$ subgroup) into simplified model topologies. This allows one to directly use the cross section upper limits or efficiency maps provided by the experimental collaborations which are provided as a function of the masses of the involved BSM particles governing the kinematics of the production and decay.[4]

So far only BSM searches for missing transverse momentum (MET) have been taken into account within SModelS. However, it has widely been recognized that well-motivated BSM theories can provide non-neutral long-lived particles (LLPs) leading to distinct signatures, often providing great sensitivity at the LHC []. In this letter we present the capabilities of SModelS 1.2 [7] to constrain such models. This version includes an additional step in the decomposition accounting for probabilities of BSM particles to decay promptly or appear long-lived and contains the signature of heavy stable charged particles (HSCPs) and R-hadrons in the database. With respect to our previous work [8] we reconsider the modeling of intermediate lifetimes which has been treated over-conservative in [8], we recast and include efficiency maps for the 13 TeV analysis [9] and add the experimental cross section upper limits for the direct production of HSCPs [9, 10] and R-hadrons [9]. Finally, SModelS 1.2 is made publicly available.[5]

We present the application to two new physics scenarios. The inert doublet model (IDM) provides one of the simplest dark matter models supplementing the standard model by just another $SU(2)$ doublet. While MET searches are scarcely sensitive to the cosmologically allowed region of parameter space, we show that for small mass splittings within the inert doublet a large range of dark matter masses can be tested.

Secondly, we consider an extension of the minimal supersymmetric standard model (MSSM) by the gravitino assuming the latter to be the lightest supersymmetric particle (LSP) and the stau to be next-to-LSP (NLSP). This is a cosmologically attractive scenario allowing to alleviate the gravitino problem and to accommodate large reheating temperatures $T_{\mathrm{R}} \sim 10^9$ GeV in the early Universe while respecting bounds from big bang nucleosynthesis (BBN) []. The complexity of the model reveals a large number of contributing topologies including R-hadron signatures relevant for both squarks and gluinos when the respective decays are 3- or 4-body suppressed. We show that the LLP results have the potential to be competitive with cosmological constraints and impact the allowed range for the reheating temperature.

[Some more refs?]

The remainder of this letter is structured as follows. In Sec. 2 we briefly describe the implementation of LLP signatures into SModelS. The application to two new physics scenarios is presented in Sec. 3. We conclude in Sec. 4. Finally, in Appendix A and Appendix B we provide details about the recasting of the HSCP analyses and a discussion about the treatment of intermediate lifetimes, respectively.

[4] A certain degree of approximation is excepted neglecting properties like the exact production mechanism and the spin of the particles in decays, see Ref. [3–6] for a corresponding discussion.

[5] http://smodels.hephy.at

3. Physics applications

In the following we use SModelS within two BSM scenarios and derive constraints on their parameter space. We consider the inert doubled model as well as a supersymmetric scenario with a gravitino LSP and a stau NLSP.

3.1. The inert doublet model

The IDM is a two-Higgs doublet model with an exact $\mathcal{Z}_2$ symmetry, under which all standard model fields (including the Higgs doublet H) are assumed to be even, while the second scalar doublet Φ is odd. It supplements the standard model Lagrangian by the gauge kinetic terms for Φ as well as additional terms in the scalar potential, which now reads

$$\begin{aligned} V = \mu_1^2|H|^2 + \mu_2^2|\Phi|^2 + \lambda_1|H|^4 + \lambda_2|\Phi|^4 \\ + \lambda_3|H|^2|\Phi|^2 + \lambda_4|H^\dagger\Phi|^2 \\ + \lambda_5/2\left[(H^\dagger\Phi)^2 + \text{h.c.}\right]. \end{aligned} \tag{1}$$

After electroweak symmetry breaking the model contains five physical scalar states with masses given by

$$\begin{aligned} m_{h^0}^2 = \mu_1^2 + 3\lambda_1 v^2\,, \quad m_{H^0}^2 = \mu_2^2 + \lambda_L v^2\,, \\ m_{A^0}^2 = \mu_2^2 + \lambda_S v^2\,, \quad m_{H^\pm}^2 = \mu_2^2 + \frac{1}{2}\lambda_3 v^2\,. \end{aligned} \tag{2}$$

where

$$\lambda_{L,S} = \frac{1}{2}\left(\lambda_3 + \lambda_4 \pm \lambda_5\right)\,, \tag{3}$$

After imposing $m_{h^0} \simeq 125.09\,\text{GeV}$ [16], we are left with five free physical parameters: m_{H^0}, m_{A^0}, $m_{H^\pm}$, λ_L and λ_2.

Despite its simplicity, the IDM leads to a rich phenomenology and provides a viable dark matter candidate with observable signatures in direct and indirect detection experiments. For recent accounts see *e.g.* [17–19]. At the LHC the IDM is extremely difficult to observe via MET searches [20–25]. For instance, a reinterpretation of dilepton plus MET signatures at the 8 TeV LHC [26] provides sensitivity up to $m_{H^0} \simeq 55\,\text{GeV}$ only [25]. However, in this low-mass region, the H^0 thermal relic density (Ω_{IDM}) is above the observed dark matter density (Ω_{CDM}). There are three regions where the IDM can account for the entire observed relic density ($55\,\text{GeV} \lesssim m_{H^0} \leq m_{h^0}/2$, $m_{H^0} \simeq 72\,\text{GeV}$ and $m_{H^0} \gtrsim 500\,\text{GeV}$) and a region where it can account only for a fraction of Ω_{CDM} ($72 \lesssim m_{H^0} \lesssim 500\,\text{GeV}$) [19, 27].

In this work we focus on the region with small mass splittings ($\Delta m = m_{H^\pm} - m_{H^0} \leq 1\,\text{GeV}$) and use SModelS 1.2 to reinterpret the LHC limits from HSCP searches within the IDM model. For this purpose we perform a scan over the IDM 5-dimensional parameter space restricted to:

$$\begin{aligned} 100\,\text{GeV} \leq &\quad m_{H^0} &\leq 1\,\text{TeV} \\ m_{H^0} < &\quad m_{A^0} &\leq 1.1\,\text{TeV} \\ 10\,\text{MeV} \leq &\quad m_{H^\pm} - m_{H^0} &\leq 1\,\text{GeV} \\ -4\pi \leq &\quad \lambda_L &\leq 4\pi \\ 10^{-6} \leq &\quad \lambda_2 &\leq 4\pi \end{aligned} \tag{4}$$

and we impose $10^{-3} \leq R \equiv \Omega_{\text{IDM}}/\Omega_{\text{CDM}} \leq 1$. In addition we take into account constraints from Higgs invisible decays [28], electroweak precision observables [29, 30], from searches for charginos and neutralinos at LEP-II [20, 31]. indirect detection limits from γ-ray observations of dwarf spheroidal galaxies [32] and theoretical constraints on unitarity, perturbativity and vacuum stability computed with 2HDMC [30] (see Ref. [19] for further details[6]). In the following we only consider points allowed within the 2σ region of the above constraints. We use the nested-sampling algorithm MultiNest [34, 35] to efficiently explore the parameter space.

For the allowed parameter space we compute the decay tables and production cross-sections with MadGraph5_aMC@NLO [36] and compute the LHC constraints with SModelS 1.2. For each parameter space point the constraining power of LHC searches can be conveniently parametrized by the ratio of the relevant signal cross-section (σ_{th}) to the corresponding analysis upper limit (σ_{UL}): $r = \sigma_{th}/\sigma_{UL}$ (see Ref. [2] for more details). If $r \geq 1$ for at least one analysis we consider the point as being excluded.

The results are shown in Fig. 1. In the left panel we display the signal strength r in the $m_{H^\pm}$-$c\tau_{H^\pm}$ plane, while the right panel shows the dark matter fraction R in the m_{H^0}-Δm plane. Although r does in principle depend on all the model parameters, we can see that it is mostly driven by the charged Higgs mass and its lifetime. We hence show an approximate exclusion curve in the plot (dark dashed curve). In all the parameter space considered we have verified that the exclusion is completely dominated by the HSCP searches and even though the SModelS MET constraints were also applied, they could not exclude any of the points. As seen in Fig. 1, in the quasi-stable limit ($c\tau \gtrsim 10^3\,\text{m}$) HSCP searches exclude $H^\pm$ masses up to 580 GeV. This limit goes beyond the 13 TeV LHC limit for direct production of detector-stable staus which reaches $m_{\tilde{\tau}} =$

[6] With respect to Ref. [19], in this work we update direct detection constraints additionally imposing the 90% CL upper limits on the spin-independent dark matter-nucleon scattering cross-section recently obtained by Xenon1T [33].

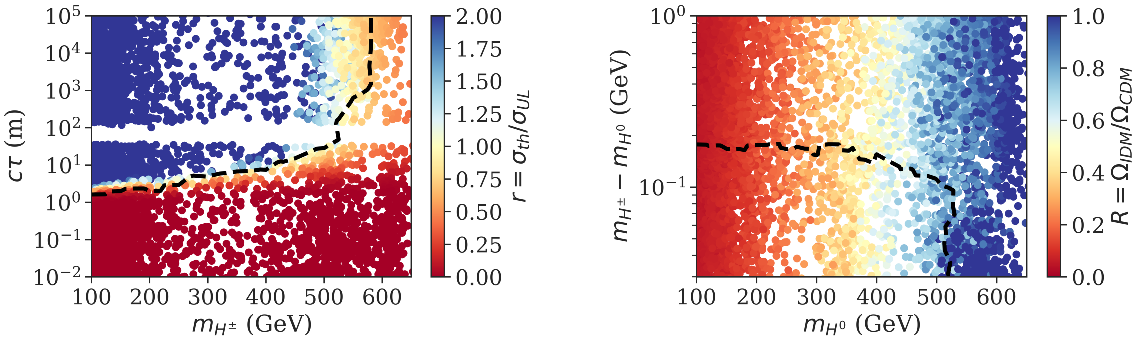

Figure 1: Allowed IDM parameter points (imposing all but the LHC constraints) in the $m_{H^\pm}$-$c\tau$ plane (left panel) and $m_{H^\pm}$-Δm (right panel). The color denotes the LHC signal strength r and the dark matter fraction R, respectively. The black dashed curve shows the (interpolated) 95% CL exclusion contour from the LHC ($r = 1$).

360 GeV [9]. The reason for the higher reach is the appearance of the additional W-mediated production channel $pp \to H^0 H^\pm$ as well as (to a lesser extend and depending on m_{A^0}) the channels $pp \to A^0 H^\pm, A^0 A^0$ with $A^0 \to H^\pm$. As an example, for $m_{H^0} \simeq m_{A^0} \simeq m_{H^0} \simeq 520$ GeV we have $\sigma(H^\pm H^\pm) + \sigma(H^\pm H^0) + \sigma(H^\pm A^0) \simeq 1.14$ fb against $\sigma(\tilde{\tau}\tilde{\tau}) \simeq 0.15$ fb [9] for the same stau mass.

At the lower edge of our scan range, for $m_{H^\pm} \simeq m_{H^0} \gtrsim 100$ GeV, HSCP searches are able to constrain decay lengths down to around $c\tau \simeq 2\,m$. Here the significant exponential suppression of $\mathcal{F}_{\text{long}}$ is compensated by the large cross-section. Note that our choice for $\langle \ell_{\text{outer}}/\gamma\beta \rangle_{\text{eff}}$ leads to a somewhat conservative exclusion limit in this part of the parameter space (see left panel of Fig. B.5 as well as the corresponding discussion in Appendix B). We point out that the calculation of $c\tau$ involves a certain degree of approximation. First, the decays are computed at leading order with MadGraph5_aMC@NLO and the decay channels with first generation quarks in the final state are turned off once Δm is smaller than the pion mass. This introduces the (artificial) gap seen at $c\tau \sim 100$ m, which would not appear if the proper phase-space including the pion mass were included.

In the right panel of Fig. 1 we show the HSCP exclusion curve in the Δm-m_{H^0} plane. As seen, the limits exclude a significant part of the parameter space with $\Delta m \lesssim 0.2$ GeV. Interestingly, the HSCP searches are starting to exclude part of the region with $R = 1$, where the IDM can account for the entire observed relic density ($m_{H^0} \gtrsim 500$ GeV). Note that disappearing track searches have the potential to further extend the reach towards larger Δm [18].

3.2. Gravitino dark matter scenario

The gravitino – the superpartner of the graviton – is an attractive dark matter candidate in supersymmetric theories [37, 38]. Models where the gravitino ($\tilde{G}$) is the LSP can alleviate the gravitino problem which appears in neutralino LSP scenarios [11–14] unless the gravitino is much heavier than the rest of the supersymmetric spectrum which in turn severely limits the viable options for supersymmetry breaking. Once the gravitino is the LSP, the lightest sparticle of the MSSM (*i.e.* the NLSP) can be any sparticle. However, in order to not reintroduce a severe problem through late decays of the NLSP – spoiling successful BBN predictions [39] – certain choices appear more promising. For instance, the stau is an attractive NLSP candidate providing a large annihilation cross-section, thus resulting in smaller freeze-out abundances. As a consequence, the impact of the late time decay $\tilde{\tau} \to \tau\tilde{G}$ on BBN is reduced. On the other hand it also reduces the contribution to the gravitino abundance through NLSP decays. This allows for a larger thermal contribution of gravitino production while not over-closing the Universe. Since the thermal contribution is (approximately) proportional to the reheating temperature, $\Omega^{\text{th}}_{\tilde{G}} \propto T_{\text{R}}$ [40–42], it allows for higher values of T_{R}, as preferred by classes of models for leptogenesis and inflation *[REFS?]*.

Here we revisit the parameter scan performed in [43, 44] refining and updating the constraints from long-lived particle searches at the LHC. The scan is performed within the framework of the pMSSM, where the additional assumption $m_{\tilde{q}_{1,2}} \equiv m_{\tilde{Q}_{1,2}} = m_{\tilde{u}_{1,2}} = m_{\tilde{d}_{1,2}}$ has been imposed. In this way we achieve a 17-dimensional parameter space with input parameters and scan ranges given by:[7]

$$\begin{array}{rcll}
-10\,\mathrm{TeV} \le & A_t & \le 10\,\mathrm{TeV} & \\
-8\,\mathrm{TeV} \le & A_b,\, A_\tau, \mu & \le 8\,\mathrm{TeV} & \\
1 \le & \tan\beta & \le 60 & \\
100\,\mathrm{GeV} \le & m_A & \le 4\,\mathrm{TeV} & \\
200\,\mathrm{GeV} \le & m_{\tilde\tau_1} & \le 2\,\mathrm{TeV} & \\
700\,\mathrm{GeV} \le & m_{\tilde t_1}, m_{\tilde b_1} & \le 5\,\mathrm{TeV} & (5)\\
0 < & \theta_{\tilde\tau}, \theta_{\tilde t} & < \pi & \\
m_{\tilde\tau_1} \le & m_{\tilde L_{1,2}}, m_{\tilde e_{1,2}} & \le 4\,\mathrm{TeV} & \\
1.2\,\mathrm{TeV} \le & m_{\tilde q_{1,2}} & \le 8\,\mathrm{TeV} & \\
m_{\tilde\tau_1} \le & M_1, M_2 & \le 4\,\mathrm{TeV} & \\
1\,\mathrm{TeV} \le & M_3 & \le 5\,\mathrm{TeV} &
\end{array}$$

The particle spectrum has been computed with SuSpect 2.41 [45] and FeynHiggs 2.9.2 [46]. Since we are interested in the gravitino LSP scenario with a stau NLSP, we have required all the points to have the lighter stau $\tilde\tau_1$ as the NLSP. In addition we have also imposed $m_h \in [123; 128]\,\mathrm{GeV}$ [16, 47].

The decay widths and branching ratios have been computed with SDecay [48, 49] and (in the case of missing dominant decay channels) MadGraph5_aMC@NLO [36], while the freeze-out abundance of staus have been computed with micrOMEGAs 2.4.5 [50]. We considered constraints on the MSSM Higgs sector *[The end of the paragraph also mentions MSSM Higgs sector constraints. Clarify?]*, performed at LEP, the Tevatron and the LHC [51] and EW precision bounds [52–54] as well as theoretical constrains arising from charge or color breaking vacua [55–60]. With respect to [43] we imposed updated flavor constraints: $\mathrm{BR}(B \to X_s\gamma) \in [3.0; 3.64] \times 10^{-4}$ [61] and $\mathrm{BR}(B_s^0 \to \mu^+\mu^-) \in [1.74; 4.34] \times 10^{-9}$ [62]. Finally, limits on the MSSM Higgs sector were included by applying the conservative constraints on m_A and $\tan\beta$ derived in the $m_h^{\mathrm{mod}+}$-scenario [63].

Since the gravitino mass can be taken as an additional free parameter, for each point in the pMSSM parameter space satisfying the above requirements, 10 gravitino masses have been generated. The randomly selected values were required to lie within an interval where the total $\tilde G$ abundance can match the measured dark matter abundance:

$$\Omega_{\tilde G}^{\text{non-th}} h^2 + \Omega_{\tilde G}^{\text{th}} h^2 = \Omega_{\text{CDM}} h^2\,, \tag{6}$$

where $\Omega_{\tilde G}^{\text{th}} h^2$ and $\Omega_{\tilde G}^{\text{non-th}} h^2$ are the thermal and non-thermal gravitino relic abundances, respectively. The latter is generated once the frozen-out $\tilde\tau$s decay to $\tilde G$s, thus enhancing the total gravitino abundance. On the other hand the thermal gravitino relic abundance is mostly determined by the reheat temperature, T_{R} [40–42]. Therefore, given a pMSSM point (and hence $\Omega_{\tilde G}^{\text{non-th}} h^2$), the reheating temperature is computed imposing (9) with $\Omega_{\text{CDM}} h^2 = 0.1189$. For each of the resulting points in the (17+1)-dimensional parameter space (that by construction fulfills the relic density constraint) constraints from BBN [64, 65][8] have been imposed (see Refs. [43, 44] for further details).

After selecting ∼26k points satisfying the above constraints, we have used SModelS 1.2 to decompose each point signal into all occurring simplified model topologies, which includes production and cascade decays of all MSSM supersymmetric particles. The LO production cross-sections have been computed using Pythia 8 [68, 69], while NLL cross-sections for $\tilde g\tilde g$, $\tilde g\tilde q$ and $\tilde q\tilde q$ have been obtained using NLLFast [70–76]. The results from the 8 TeV and 13 TeV HSCP and R-hadron searches were then applied in order to constrain the points. Since all the cascade decays terminate at the stau NLSP (at collider scales), MET constraints do not apply. From all the tested points, ∼ 5k are excluded and ∼ 21k are allowed, as shown in Fig. 2. For a fixed gravitino mass (below ∼ 200 GeV), the largest values of T_{R} are excluded by the LHC constraints. This is due to the fact that the largest reheat temperatures are typically achieved for points with small

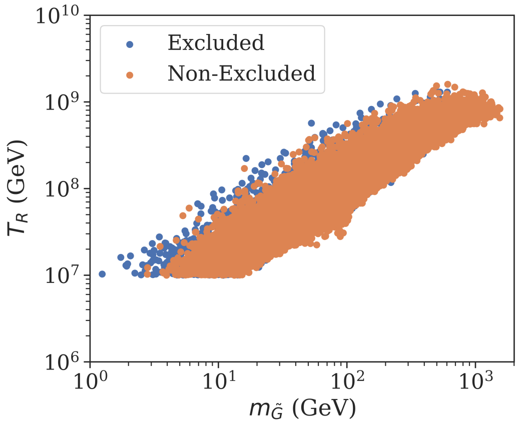

Figure 2: Effect of the LHC exclusion bounds on the otherwise allowed points in the plane spanned by the gravitino mass and reheating temperature.

[7] In this phenomenologically driven parameter scan the spectrum parameters of the third generation sfermions, $m_{\tilde\tau_1}$, $m_{\tilde t_1}$, $m_{\tilde b_1}$, $\theta_{\tilde\tau}$ and $\theta_{\tilde t}$, were chosen as input parameters in order to obtain an equally good coverage of small and large mixing scenarios. Tree-level relations were used to translate these parameters into soft parameters. In the further analysis only the values recalculated by the spectrum generator are used consistently.

[8] Furthermore, constraints from diffuse gamma ray observations [66, 67] have been considered, which, however, have found to be much less relevant [44].

gluino masses*[Explain more?]*, which in turn contain large production cross-sections at the LHC. As a result these points can be probed by the HSCP and R-hadron searches. We see, however, that the largest values of $T_{\rm R}$ ($\simeq 10^9$ GeV) obtained in the scan are still allowed by the LHC constraints obtained with SModelS.

In order to discuss which searches and topologies are relevant for testing the gravitino scenario, we show in Fig. 3 a histogram for the number of excluded points as a function of the gluino mass. In the left panel the number of excluded points is grouped according to which is the most constraining type of signature. The stacked histogram shows that the bulk of the points are excluded by topologies containing HSCP signatures, as expected. Nonetheless a significant fraction of points at low $m_{\tilde{g}}$ are excluded by R-hadron constrains for long-lived gluinos. These points typically have heavy squarks, resulting in suppressed 3-body or 4-body gluino decays. In a similar way, points with light squarks and heavy gauginos and higgsinos lead to long-lived squarks which can also be constrained by the R-hadron searches, as shown by the orange histogram. In order to illustrate the constraining power of combining results for multiple simplified model topologies, we also display (dark blue histogram) the distribution of excluded points obtained using only the CMS limits for pair production of long-lived staus, gluinos and squarks. As it can be seen, the number of excluded points in this case (~ 200) is drastically reduced when compared to the one obtained with all the topologies included in SModelS.

We point out, however, that the constraining power of SModelS is still limited by the number of simplified model results contained in its database. The points from the pMSSM scan performed here display a large variety of topologies and many of them do not fall within the 8 HSCP or the 2 R-hadron topologies included in the database. However SModelS can also be used to identify the most relevant missing topologies [1, 2, 77]. In the right panel of Fig. 3 we show the non-excluded points with a total SUSY production cross-section (at 13 TeV) larger than 5 fb. Due to their sizeable cross-section, such points have a potential for being excluded by the HSCP or R-hadron searches. The stacked histogram shows the distribution of non-excluded points as a function of the gluino mass grouped according to the missing topology with largest weight (cross-section times branching ratio). Most of the points have $m_{\tilde{g}} < 1.7$ TeV, since this ensures $\sigma(\tilde{g}\tilde{g}) \gtrsim 5$ fb. The almost flat distribution at large $m_{\tilde{g}}$ corresponds to points with light squarks in the spectrum, thus also resulting in large total cross-sections. We see that the missing topology which occurs more often in Fig. 3 (light blue histogram) corresponds to pair production of BSM particles, which then go through 4-body decays to the HSCP. This topology is mostly generated by points with very light gluinos, which then decay directly to the $\tilde{\tau}$ through 4-body decays. Furthermore, we see that topologies with 1-step decays to R-hadrons (green and dark red histograms) can also be potentially powerful when constraining this scenario. These topologies often appear in points with light quarks (gluinos) which decay to long-lived gluinos (quarks).

4. Conclusion

In this work we have applied SModelS 1.2 to constrain two new physics scenarios containing long-lived particles. This latest SModelSversion is capable to test BSM models that contain non-neutral long-lived BSM particles. We have implemented HSCP and R-hadron searches at the 8 and 13 TeV LHC. We discuss to benchmark scenarios in order to illustrate its capabilities, the IDM and a gravitino dark matter scenario.

[...]

Acknowledgements

We would like to thank Nishita Desai, Suchita Kulkarni and Wolfgang Waltenberger for very helpful discussions.

This work is supported by the German Research Foundation DFG through the research unit "New physics at the LHC". A.L. is supported by the Sao Paulo Research Foundation (FAPESP), projects 2015/20570-1 and 2016/50338-6. *[S. Kraml is...]*

Appendix A. Recasting and validation

In this appendix we detail the recasting of the 8 and 13 TeV HSCP searches used in SModelS. We first review the recasting for the 8 TeV CMS HSCP analysis presented in [10]. The authors of [10] provide signature efficiencies for the off- and online selection criteria, $P_{\rm on}(\boldsymbol{k})$ and $P_{\rm off}(\boldsymbol{k})$, respectively, as a function of the generator-level kinematics, $\boldsymbol{k} = (\eta, p_{\rm T}, \beta)$, of isolated[9] HSCP candidates. The signal efficiency for a given parameter point can be computed from the generated events:

$$(\mathcal{A}\epsilon) = \frac{1}{N}\sum_{i=1}^{N}\mathcal{P}^{i}_{\rm event} \quad \text{(A.1)}$$

[9]Details on the imposed isolation criteria can be found in [8, 10].

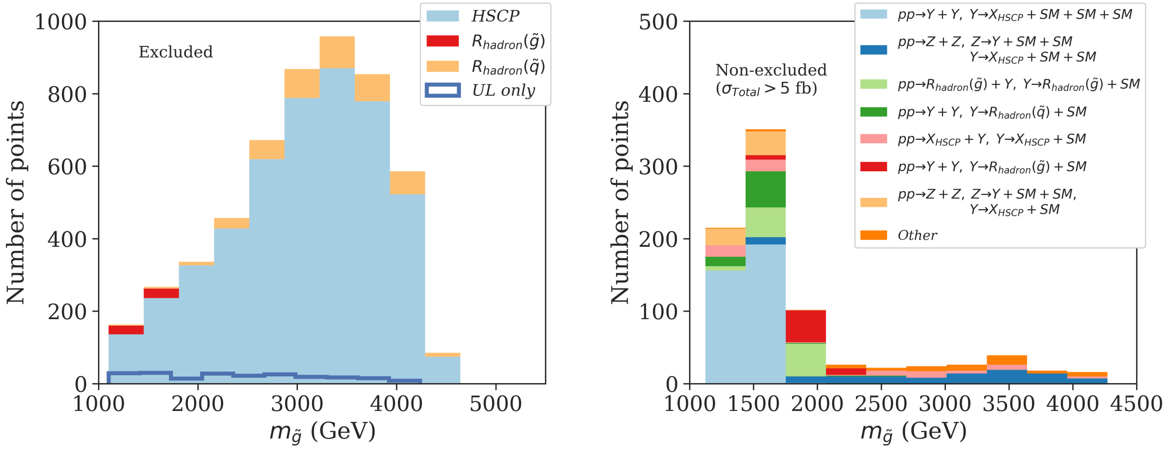

Figure 3: Left panel: Number of excluded points as a function of the gluino mass. The color indicates the most constraining type of signature. The solid blue histogram displays the number of points excluded when imposing only the CMS limits on the direct pair production of HSCPs and R-hadrons. Right panel: Number of non-excluded points with a total SUSY production cross-section of more than 5 fb at 13 TeV. The color indicates the simplified model topology with largest weight (cross-section times branching ratio).

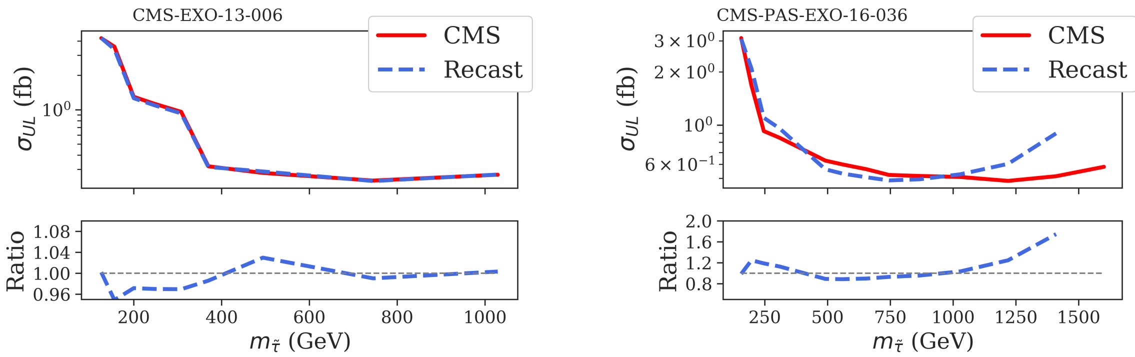

Figure A.4: Validation of the 8 TeV (left panel) and 13 TeV (right panel) CMS analysis for direct production of staus. The red and blue dashed curves show the respective cross-section upper limits from CMS and from our recast.

where the sum runs over all N events and

$$\mathcal{P}^i_{\text{event}} = \mathcal{P}^i_{\text{on}} \times \mathcal{P}^i_{\text{off}} \tag{A.2}$$

with

$$\begin{aligned}\mathcal{P}^i_{\text{on/off}} &= P_{\text{on/off}}(\boldsymbol{k}^i_1) + P_{\text{on/off}}(\boldsymbol{k}^i_2) \\ &\quad - P_{\text{on/off}}(\boldsymbol{k}^i_1) \times P_{\text{on/off}}(\boldsymbol{k}^i_2)\,.\end{aligned} \tag{A.3}$$

For one HSCP candidate in an event the formula holds with $P_{\text{on/off}}(\boldsymbol{k}^i_2) = 0$.

Using the efficiencies computed using A.1 for the direct pair production of staus and the observed and expected number of background events (along with its error) from Ref.[10] we obtain upper limits for the stau cross-section as a function of the stau mass. These can then be directly compared to the CMS values presented in Ref.[10]. The left panel of figure A.4 shows the CMS and our results for the cross-section upper limits as well as their ratio (lower frame). As we can see, the difference is always below 5% and compatible with Monte Carlo errors. Hence we expect that recasting uncertainties for the efficiencies computed with the above method and included in the SModelS database should only be of a few percent.

For the respective 13 TeV analysis [9], however, such a recast has not yet been provided. Nonetheless, since the trigger and selection criteria of the 8 and 13 TeV analyses are very similar, we expect that the signal efficiencies from the 8 TeV search do not differ drastically from the 13 TeV ones. The two analyses only differ in a slightly stronger cut on the ionization loss and time-of-flight, which effectively amounts to a slightly stronger cut on the HSCP velocity in the latter analysis.[10] Ref. [78] reported an attempt to model the 13 TeV signature efficiencies by multiplying the 8 TeV ones with a velocity dependent

[10]The effect of slightly stronger cut on p_T [9] is found to be negligible for masses of a few hundred GeV.

correction function fitted in order to resemble the signal efficiencies reported in [9]. On top of the slight reduction of the signature efficiencies for high velocities this study revealed a better performance of the CMS detector in the region of low velocities leading to larger signal efficiencies for large HSCP masses. This latter feature could, however, not be described by a universal velocity dependent correction function for direct pair production and inclusive production. In order for a proper understanding of the differences between Runs 1 and 2, further information (which is not publicly available) is needed. Therefore we choose to follow a conservative approach taking into account the reduction in the efficiency due to the slightly stronger cuts on the velocity of the HSCP candidate. We model this by multiplying $P_{\rm off}(\boldsymbol{k})$ with a correction function which is assumed to depend only on β:

$$f^{\rm corr}_{(a,b)}(\beta) = \left(1 + {\rm e}^{a(\beta - b)}\right)^{-1} \leq 1 \qquad \text{(A.4)}$$

We determine the parameters a, b in a global fit to the signal efficiencies for the pair production and inclusive production model reported in Ref. [9]. To this end we define the χ^2 function:

$$\chi^2 = \sum_m \frac{\left((\mathcal{A}\epsilon)^m_{(a,b)} - (\mathcal{A}\epsilon)^m_{\rm CMS}\right)^2}{\sigma^2_{\mathcal{A}\epsilon}} \,, \qquad \text{(A.5)}$$

where $(\mathcal{A}\epsilon)^m_{(a,b)}$ is the signal efficiency for a mass point m of the considered model using the signature efficiencies with the correction function $f^{\rm corr}_{(a,b)}$ and $(\mathcal{A}\epsilon)^m_{\rm CMS}$ is the respective signal efficiency reported by CMS in Ref. [9]. The characteristic size of the uncertainty, $\sigma_{\mathcal{A}\epsilon}$, is (arbitrarily) set to 0.02, which roughly reflects the precision of the recasting we aim at. We minimize the χ^2 using MultiNest [34, 35] and obtain the best-fit parameters: $a \simeq 500$ and $b = 0.807$. This fit was obtained using all the 12 benchmark points (6 for direct stau production and 6 for inclusive production) considered in Ref.[9] and for which signal efficiencies were reported. However, we have verified that very similar results are obtained when using only a subset of the benchmark points. Once again we compare the upper limits for the total stau direct production cross-section obtained using our recast procedure and the ones reported by CMS. The comparison is shown by the right panel of Fig. A.4, where see that, despite having a worse agreement than the 8 TeV results, the 13 TeV upper limits are within 20% while for large range of stau masses. Only for $m_{\tilde{\tau}} \gtrsim 1.2$ TeV the recasting significantly diverges from the official values. We point out, however, that the results are still conservative due to the above mentioned effects.

Appendix B. Finite lifetimes

Although the HSCP searches considered here are aimed for detector-stable particles they can also constrain models with intermediate decay length of the order of the detector size where only a certain fraction of particles decay after traversing the entire sensitive detector. In this case the fraction of long-lived particles, $\mathcal{F}_{\rm long}$, may be significantly smaller than one and the resulting signal efficiency becomes sensitive to value chosen for $L_{eff} \equiv \langle \ell_{\rm outer}/\gamma\beta \rangle_{\rm eff}$ (see eq.3). Here we discuss in detail what are the expected values for L_{eff} and justify our choice, $L_{eff} = 7$ m, used in the results presented in Sec.3 and implemented in SModelS 1.2.

The precise value of $\mathcal{F}_{\rm long}$ (and hence L_{eff}) actually depends on the input model and experimental analysis and requires a full Monte Carlo simulation for each model point in order to determine the boost distribution of the HSCP particles. However, since SModelS aims for a fast (although approximate) computation of LHC constraints for a large variety of BSM models, our goal is to determine an average value for L_{eff} which can approximately reproduce the correct value of $\mathcal{F}_{\rm long}$ obtained from a full simulation. Before we can justify this approximation, we must first discuss how to obtain $\mathcal{F}_{\rm long}$ from the full simulation for a given input model.

We first define the probability for a (metastable) particle with momentum $\boldsymbol{k}$ to decay outside the detector in a given event:

$$F_{\rm long}(\boldsymbol{k}) = \exp\left(-\frac{\ell_{\rm outer}(|\eta|)}{\gamma\beta}\frac{1}{c\tau}\right) . \qquad \text{(B.1)}$$

Here $\gamma = (1-\beta^2)^{-1/2}$ and $\ell_{\rm outer}(|\eta|)$ is the travel length through the CMS detector which we approximate by considering a cylindrical volume with radius of 7.4 m and length of 10.8 m. Using now the off- and online efficiencies ($P_{\rm on}$ and $P_{\rm off}$) discussed in Appendix A, we can extend the signal efficiency calculation from eq. (A.1) to the case of finite lifetimes using:

$$\begin{aligned}\mathcal{P}^i_{\rm event} = {} & F_{\rm long}(\boldsymbol{k}^i_1) P_{\rm on}(\boldsymbol{k}^i_1) P_{\rm off}(\boldsymbol{k}^i_1)\left(1 - F_{\rm long}(\boldsymbol{k}^i_2)\right) \\ & + F_{\rm long}(\boldsymbol{k}^i_2) P_{\rm on}(\boldsymbol{k}^i_2) P_{\rm off}(\boldsymbol{k}^i_2)\left(1 - F_{\rm long}(\boldsymbol{k}^i_1)\right) \\ & + F_{\rm long}(\boldsymbol{k}^i_1) F_{\rm long}(\boldsymbol{k}^i_2) \mathcal{P}^i_{\rm on}\mathcal{P}^i_{\rm off},\end{aligned} \qquad \text{(B.2)}$$

where $F_{\rm long}(\boldsymbol{k}^i_j)$ is the decay probability from eq.B.1 for the j-th particle in the i-th event.

Using eqs.B.2 and A.1 we can then compute the total signal efficiency for a given input model taking into account the correct finite lifetime suppression factor. This factor can then be compared

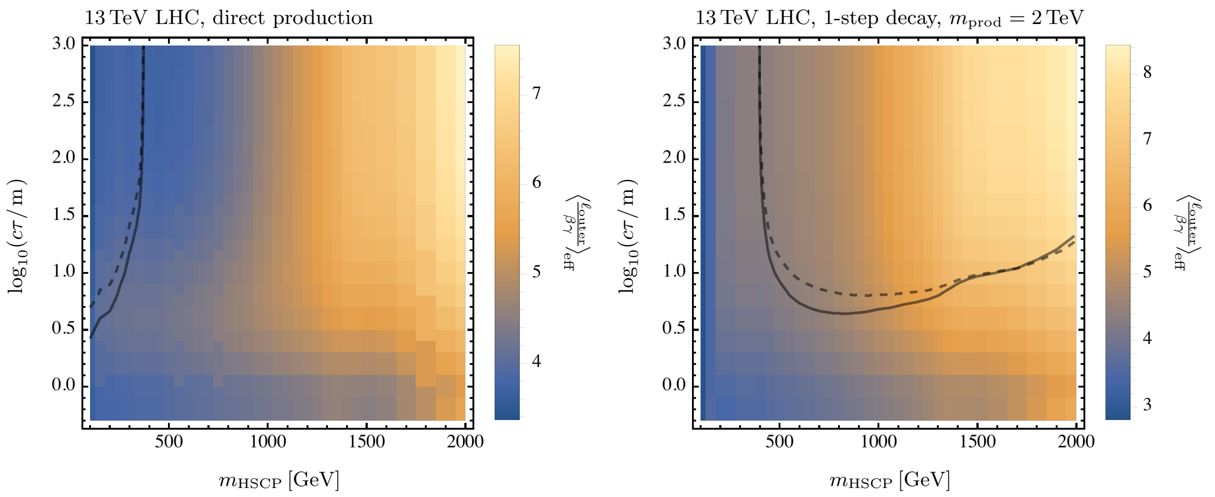

Figure B.5: The effective characteristic travel length, $\langle \ell_{\text{outer}}/\gamma\beta \rangle_{\text{eff}}$ (see text for details) in the parameter plane spanned by the HSCP mass, m_{HSCP}, and its proper decay length, $c\tau$ for direct production (left panel) and for the 1-step decay topology where we choose $m_{\text{prod}} = 2\,\text{TeV}$ for the mass of the produced mother particle (right panel). The solid and dashed curves denote the 95% CL exclusion for the event-based computation of $\ell/\gamma\beta$ and for the approximation choosing $\langle \ell_{\text{outer}}/\gamma\beta \rangle_{\text{eff}} = 7\,\text{m}$ (see text for details). For the direct production we choose the cross-section Drell-Yan stau pair production, while the cross-section for 1-step decay corresponds to (degenerate) squark production with $m_{\tilde{q}} = m_{\tilde{g}}$.

to the efficiency computed with SModelS using $\mathcal{F}_{\text{long}}$ to extract the precise value for L_{eff} given a specific input model. In Figure B.5 we consider the direct production of staus (left panel) and direct production of squarks and gluinos followed by a 1-step decay to staus at the 13 TeV LHC. In both models we vary the stau mass and lifetime, with $m_{\tilde{g}} = m_{\tilde{q}} = 2$ TeV for the second model. The color of each point in the plane shows the correct value for $L_{eff} = \langle \ell_{\text{outer}}/\gamma\beta \rangle_{\text{eff}}$ which should be used in SModelS in order for the SModelS signal efficiencies to exactly match the full simulation values. As we can see, L_{eff} does not vary significantly, spanning values within the interval ∼4-8 m. Therefore, in order to remain conservative and avoid (significantly) underestimating the signal efficiency we choose $L_{eff} = 7\ m$ (or $l_{\text{outer}} = 10$ m and $\gamma\beta = 1.3$). Using this choice we show in Fig. B.5 the corresponding exclusion curves obtained with SModelS as dashed lines. We also display the corresponding curves obtained using the full simulation. Although the SModelS curves are conservative, we see that they agree quite well with the full simulation in most of the parameter space. We therefore concluded that using a fixed $L_{eff} = 7$ m value is a valid approximation.

References

[1] S. Kraml, S. Kulkarni, U. Laa, A. Lessa, W. Magerl, D. Proschofsky-Spindler, and W. Waltenberger, *SModelS: a tool for interpreting simplified-model results from the LHC and its application to supersymmetry.* Eur. Phys. J. **C74** (2014) 2868, `arXiv:1312.4175 [hep-ph]`.

[2] F. Ambrogi, S. Kraml, S. Kulkarni, U. Laa, A. Lessa, V. Magerl, J. Sonneveld, M. Traub, and W. Waltenberger, *SModelS v1.1 user manual: Improving simplified model constraints with efficiency maps.* Comput. Phys. Commun. **227** (2018) 72–98, `arXiv:1701.06586 [hep-ph]`.

[3] L. Edelhäuser, J. Heisig, M. Krämer, L. Oymanns, and J. Sonneveld, *Constraining supersymmetry at the LHC with simplified models for squark production.* JHEP **12** (2014) 022, `arXiv:1410.0965 [hep-ph]`.

[4] L. Edelhäuser, M. Krämer, and J. Sonneveld, *Simplified models for same-spin new physics scenarios.* JHEP **04** (2015) 146, `arXiv:1501.03942 [hep-ph]`.

[5] C. Arina, M. E. C. Catalan, S. Kraml, S. Kulkarni, and U. Laa, *Constraints on sneutrino dark matter from LHC Run 1.* JHEP **05** (2015) 142, `arXiv:1503.02960 [hep-ph]`.

[6] S. Kraml, U. Laa, L. Panizzi, and H. Prager, *Scalar versus fermionic top partner interpretations of $t\bar{t} + E_T^{\text{miss}}$ searches at the LHC.* JHEP **11** (2016) 107, `arXiv:1607.02050 [hep-ph]`.

[7] F. Ambrogi, J. Heisig, S. Kraml, S. Kulkarni, U. Laa, A. Lessa, H. Reyes-Gonzalez, and W. Waltenberger, *SModelS v1.2 release note, in preparation.*

[8] J. Heisig, A. Lessa, and L. Quertenmont, *Simplified Models for Exotic BSM Searches.* JHEP **12** (2015) 087, `arXiv:1509.00473 [hep-ph]`.

[9] **CMS** Collaboration, V. Khachatryan *et al.*, *Search for heavy stable charged particles with* 12.9 fb^{-1} *of 2016 data,* Tech. Rep. CMS-PAS-EXO-16-036, 2016. `http://cds.cern.ch/record/2205281`.

[10] **CMS** Collaboration, V. Khachatryan *et al.*, *Constraints on the pMSSM, AMSB model and on other models from the search for long-lived charged particles in proton-proton collisions at sqrt(s) = 8 TeV.* Eur. Phys. J. **C75** (2015) no. 7, 325, `arXiv:1502.02522 [hep-ex]`.

[11] S. Weinberg, *Cosmological Constraints on the Scale of Supersymmetry Breaking.* Phys. Rev. Lett. **48** (1982) 1303.

[12] J. R. Ellis, J. E. Kim, and D. V. Nanopoulos,

Cosmological Gravitino Regeneration and Decay. Phys. Lett. **B145** (1984) 181.
[13] I. V. Falomkin, G. B. Pontecorvo, M. G. Sapozhnikov, M. Y. Khlopov, F. Balestra, and G. Piragino, *Low-energy $\bar{p}\,^4He$ Annihilation And Problems Of The Modern Cosmology, GUT And SUSY Models*. Nuovo Cim. **A79** (1984) 193–204. [Yad. Fiz. **39** (1984), 990].
[14] J. R. Ellis, D. V. Nanopoulos, and S. Sarkar, *The Cosmology of Decaying Gravitinos*. Nucl. Phys. **B259** (1985) 175.
[15] **CMS** Collaboration, S. Chatrchyan *et al.*, *Searches for long-lived charged particles in pp collisions at $\sqrt{s}$=7 and 8 TeV*. JHEP **07** (2013) 122, `arXiv:1305.0491 [hep-ex]`.
[16] **Particle Data Group** Collaboration, K. A. Olive *et al.*, *Review of Particle Physics*. Chin. Phys. **C38** (2014) 090001.
[17] A. Ilnicka, M. Krawczyk, and T. Robens, *Inert Doublet Model in light of LHC Run I and astrophysical data*. Phys. Rev. **D93** (2016) no. 5, 055026, `arXiv:1508.01671 [hep-ph]`.
[18] A. Belyaev, G. Cacciapaglia, I. P. Ivanov, F. Rojas-Abatte, and M. Thomas, *Anatomy of the Inert Two Higgs Doublet Model in the light of the LHC and non-LHC Dark Matter Searches*. Phys. Rev. **D97** (2018) no. 3, 035011, `arXiv:1612.00511 [hep-ph]`.
[19] B. Eiteneuer, A. Goudelis, and J. Heisig, *The inert doublet model in the light of Fermi-LAT gamma-ray data: a global fit analysis*. Eur. Phys. J. **C77** (2017) no. 9, 624, `arXiv:1705.01458 [hep-ph]`.
[20] A. Pierce and J. Thaler, *Natural Dark Matter from an Unnatural Higgs Boson and New Colored Particles at the TeV Scale*. JHEP **0708** (2007) 026, `arXiv:hep-ph/0703056 [HEP-PH]`.
[21] Q.-H. Cao, E. Ma, and G. Rajasekaran, *Observing the Dark Scalar Doublet and its Impact on the Standard-Model Higgs Boson at Colliders*. Phys. Rev. D **76** (2007) 095011, `arXiv:0708.2939 [hep-ph]`.
[22] E. Dolle, X. Miao, S. Su, and B. Thomas, *Dilepton Signals in the Inert Doublet Model*. Phys. Rev. D **81** (2010) 035003, `arXiv:0909.3094 [hep-ph]`.
[23] X. Miao, S. Su, and B. Thomas, *Trilepton Signals in the Inert Doublet Model*. Phys. Rev. D **82** (2010) 035009, `arXiv:1005.0090 [hep-ph]`.
[24] M. Gustafsson, S. Rydbeck, L. Lopez-Honorez, and E. Lundstrom, *Status of the Inert Doublet Model and the Role of multileptons at the LHC*. Phys.Rev. **D86** (2012) 075019, `arXiv:1206.6316 [hep-ph]`.
[25] G. Belanger, B. Dumont, A. Goudelis, B. Herrmann, S. Kraml, and D. Sengupta, *Dilepton constraints in the Inert Doublet Model from Run 1 of the LHC*. Phys. Rev. **D91** (2015) no. 11, 115011, `arXiv:1503.07367 [hep-ph]`.
[26] **ATLAS** Collaboration, G. Aad *et al.*, *Search for direct production of charginos, neutralinos and sleptons in final states with two leptons and missing transverse momentum in pp collisions at $\sqrt{s} = 8$ TeV with the ATLAS detector*. JHEP **05** (2014) 071, `arXiv:1403.5294 [hep-ex]`.
[27] A. Goudelis, B. Herrmann, and O. Stål, *Dark matter in the Inert Doublet Model after the discovery of a Higgs-like boson at the LHC*. JHEP **09** (2013) 106, `arXiv:1303.3010 [hep-ph]`.
[28] **ATLAS** Collaboration, G. Aad *et al.*, *Constraints on new phenomena via Higgs boson couplings and invisible decays with the ATLAS detector*. JHEP **11** (2015) 206, `arXiv:1509.00672 [hep-ex]`.
[29] **Gfitter Group** Collaboration, M. Baak, J. Cuth, J. Haller, A. Hoecker, R. Kogler, K. Mönig, M. Schott, and J. Stelzer, *The global electroweak fit at NNLO and prospects for the LHC and ILC*. Eur. Phys. J. **C74** (2014) 3046, `arXiv:1407.3792 [hep-ph]`.
[30] D. Eriksson, J. Rathsman, and O. Stal, *2HDMC: Two-Higgs-Doublet Model Calculator Physics and Manual*. Comput. Phys. Commun. **181** (2010) 189–205, `arXiv:0902.0851 [hep-ph]`.
[31] E. Lundström, M. Gustafsson, and J. Edsjö, *The Inert Doublet Model and LEP II Limits*. Phys. Rev. D **79** (2009) 035013, `arXiv:0810.3924 [hep-ph]`.
[32] **DES, Fermi-LAT** Collaboration, A. Albert *et al.*, *Searching for Dark Matter Annihilation in Recently Discovered Milky Way Satellites with Fermi-LAT*. `arXiv:1611.03184 [astro-ph.HE]`.
[33] **XENON** Collaboration, E. Aprile *et al.*, *Dark Matter Search Results from a One Tonne$\times$Year Exposure of XENON1T*. `arXiv:1805.12562 [astro-ph.CO]`.
[34] F. Feroz, M. P. Hobson, and M. Bridges, *MultiNest: an efficient and robust Bayesian inference tool for cosmology and particle physics*. Mon. Not. Roy. Astron. Soc. **398** (2009) 1601–1614, `arXiv:0809.3437 [astro-ph]`.
[35] F. Feroz, M. P. Hobson, E. Cameron, and A. N. Pettitt, *Importance Nested Sampling and the MultiNest Algorithm*. `arXiv:1306.2144 [astro-ph.IM]`.
[36] J. Alwall, R. Frederix, S. Frixione, V. Hirschi, F. Maltoni, O. Mattelaer, H. S. Shao, T. Stelzer, P. Torrielli, and M. Zaro, *The automated computation of tree-level and next-to-leading order differential cross sections, and their matching to parton shower simulations*. JHEP **07** (2014) 079, `arXiv:1405.0301 [hep-ph]`.
[37] P. Fayet, "Experimental consequences of supersymmetry," in *Proceedings of the XVIth Rencontre de Moriond*, J. Tran Thanh Van, ed., vol. 1, pp. 347–367. Editions Frontieres, 1981.
[38] H. Pagels and J. R. Primack, *Supersymmetry, Cosmology and New TeV Physics*. Phys. Rev. Lett. **48** (1982) 223.
[39] T. Moroi, H. Murayama, and M. Yamaguchi, *Cosmological constraints on the light stable gravitino*. Phys. Lett. **B303** (1993) 289–294.
[40] M. Bolz, W. Buchmuller, and M. Plumacher, *Baryon asymmetry and dark matter*. Phys. Lett. **B443** (1998) 209–213, `arXiv:hep-ph/9809381 [hep-ph]`.
[41] M. Bolz, A. Brandenburg, and W. Buchmuller, *Thermal production of gravitinos*. Nucl. Phys. **B606** (2001) 518–544, `arXiv:hep-ph/0012052 [hep-ph]`. [Erratum: Nucl. Phys.B790,336(2008)].
[42] J. Pradler and F. D. Steffen, *Constraints on the Reheating Temperature in Gravitino Dark Matter Scenarios*. Phys. Lett. **B648** (2007) 224–235, `arXiv:hep-ph/0612291 [hep-ph]`.
[43] J. Heisig, J. Kersten, B. Panes, and T. Robens, *A survey for low stau yields in the MSSM*. JHEP **04** (2014) 053, `arXiv:1310.2825 [hep-ph]`.
[44] J. Heisig, *Gravitino LSP and leptogenesis after the first LHC results*. JCAP **1404** (2014) 023, `arXiv:1310.6352 [hep-ph]`.
[45] A. Djouadi, J.-L. Kneur, and G. Moultaka, *SuSpect: A Fortran code for the supersymmetric and Higgs particle spectrum in the MSSM*. Comput. Phys. Commun. **176** (2007) 426–455, `arXiv:hep-ph/0211331 [hep-ph]`.
[46] S. Heinemeyer, W. Hollik, and G. Weiglein, *FeynHiggs: A Program for the calculation of the*

masses of the neutral CP even Higgs bosons in the MSSM. Comput. Phys. Commun. **124** (2000) 76–89, arXiv:hep-ph/9812320 [hep-ph].

[47] G. Degrassi, S. Heinemeyer, W. Hollik, P. Slavich, and G. Weiglein, *Towards high precision predictions for the MSSM Higgs sector*. Eur. Phys. J. **C28** (2003) 133–143, arXiv:hep-ph/0212020 [hep-ph].

[48] A. Djouadi, M. M. Muhlleitner, and M. Spira, *Decays of supersymmetric particles: The Program SUSY-HIT (SUspect-SdecaY-Hdecay-InTerface)*. Acta Phys. Polon. **B38** (2007) 635–644, arXiv:hep-ph/0609292 [hep-ph].

[49] S. Kraml and D. T. Nhung, *Three-body decays of sleptons in models with non-universal Higgs masses*. JHEP **02** (2008) 061, arXiv:0712.1986 [hep-ph].

[50] G. Belanger, F. Boudjema, A. Pukhov, and A. Semenov, *Dark matter direct detection rate in a generic model with micrOMEGAs 2.2*. Comput. Phys. Commun. **180** (2009) 747–767, arXiv:0803.2360 [hep-ph].

[51] P. Bechtle, O. Brein, S. Heinemeyer, G. Weiglein, and K. E. Williams, *HiggsBounds 2.0.0: Confronting Neutral and Charged Higgs Sector Predictions with Exclusion Bounds from LEP and the Tevatron*. Comput. Phys. Commun. **182** (2011) 2605–2631, arXiv:1102.1898 [hep-ph].

[52] **CDF, D0** Collaboration, T. E. W. Group, *2012 Update of the Combination of CDF and D0 Results for the Mass of the W Boson*. arXiv:1204.0042 [hep-ex].

[53] P. Bechtle, S. Heinemeyer, O. Stal, T. Stefaniak, G. Weiglein, and L. Zeune, *MSSM Interpretations of the LHC Discovery: Light or Heavy Higgs?* Eur. Phys. J. **C73** (2013) no. 4, 2354, arXiv:1211.1955 [hep-ph].

[54] S. Heinemeyer, W. Hollik, D. Stockinger, A. M. Weber, and G. Weiglein, *Precise prediction for M(W) in the MSSM*. JHEP **08** (2006) 052, arXiv:hep-ph/0604147 [hep-ph].

[55] T. Kitahara and T. Yoshinaga, *Stau with Large Mass Difference and Enhancement of the Higgs to Diphoton Decay Rate in the MSSM*. JHEP **05** (2013) 035, arXiv:1303.0461 [hep-ph].

[56] J. M. Frere, D. R. T. Jones, and S. Raby, *Fermion Masses and Induction of the Weak Scale by Supergravity*. Nucl. Phys. **B222** (1983) 11–19.

[57] L. Alvarez-Gaume, J. Polchinski, and M. B. Wise, *Minimal Low-Energy Supergravity*. Nucl. Phys. **B221** (1983) 495.

[58] M. Claudson, L. J. Hall, and I. Hinchliffe, *Low-Energy Supergravity: False Vacua and Vacuous Predictions*. Nucl. Phys. **B228** (1983) 501–528.

[59] C. Kounnas, A. B. Lahanas, D. V. Nanopoulos, and M. Quiros, *Low-Energy Behavior of Realistic Locally Supersymmetric Grand Unified Theories*. Nucl. Phys. **B236** (1984) 438–466.

[60] J. P. Derendinger and C. A. Savoy, *Quantum Effects and SU(2) x U(1) Breaking in Supergravity Gauge Theories*. Nucl. Phys. **B237** (1984) 307–328.

[61] **HFLAV** Collaboration, Y. Amhis *et al.*, *Averages of b-hadron, c-hadron, and τ-lepton properties as of summer 2016*. Eur. Phys. J. **C77** (2017) no. 12, 895, arXiv:1612.07233 [hep-ex].

[62] **LHCb** Collaboration, R. Aaij *et al.*, *Measurement of the $B_s^0 \to \mu^+\mu^-$ branching fraction and effective lifetime and search for $B^0 \to \mu^+\mu^-$ decays*. Phys. Rev. Lett. **118** (2017) no. 19, 191801, arXiv:1703.05747 [hep-ex].

[63] **CMS** Collaboration, A. M. Sirunyan *et al.*, *Search for additional neutral MSSM Higgs bosons in the $\tau\tau$ final state in proton-proton collisions at $\sqrt{s} = 13$ TeV*. arXiv:1803.06553 [hep-ex].

[64] K. Jedamzik, *Bounds on long-lived charged massive particles from Big Bang nucleosynthesis*. JCAP **0803** (2008) 008, arXiv:0710.5153 [hep-ph].

[65] K. Jedamzik, *Big bang nucleosynthesis constraints on hadronically and electromagnetically decaying relic neutral particles*. Phys. Rev. **D74** (2006) 103509, arXiv:hep-ph/0604251 [hep-ph].

[66] P. Sreekumar, F. W. Stecker, and S. C. Kappadath, *The extragalactic diffuse gamma-ray emission*. AIP Conf. Proc. **410** (1997) no. 1, 344, arXiv:astro-ph/9709258 [astro-ph].

[67] G. D. Kribs and I. Z. Rothstein, *Bounds on longlived relics from diffuse gamma-ray observations*. Phys. Rev. **D55** (1997) 4435–4449, arXiv:hep-ph/9610468 [hep-ph]. [Erratum: Phys. Rev.D56,1822(1997)].

[68] T. Sjostrand, S. Mrenna, and P. Z. Skands, *PYTHIA 6.4 Physics and Manual*. JHEP **0605** (2006) 026, arXiv:hep-ph/0603175 [hep-ph].

[69] T. Sjöstrand, S. Ask, J. R. Christiansen, R. Corke, N. Desai, P. Ilten, S. Mrenna, S. Prestel, C. O. Rasmussen, and P. Z. Skands, *An Introduction to PYTHIA 8.2*. Comput. Phys. Commun. **191** (2015) 159–177, arXiv:1410.3012 [hep-ph].

[70] W. Beenakker, R. Hopker, M. Spira, and P. M. Zerwas, *Squark and gluino production at hadron colliders*. Nucl. Phys. **B492** (1997) 51–103, arXiv:hep-ph/9610490 [hep-ph].

[71] W. Beenakker, M. Kramer, T. Plehn, M. Spira, and P. M. Zerwas, *Stop production at hadron colliders*. Nucl. Phys. **B515** (1998) 3–14, arXiv:hep-ph/9710451 [hep-ph].

[72] A. Kulesza and L. Motyka, *Threshold resummation for squark-antisquark and gluino-pair production at the LHC*. Phys. Rev. Lett. **102** (2009) 111802, arXiv:0807.2405 [hep-ph].

[73] A. Kulesza and L. Motyka, *Soft gluon resummation for the production of gluino-gluino and squark-antisquark pairs at the LHC*. Phys. Rev. **D80** (2009) 095004, arXiv:0905.4749 [hep-ph].

[74] W. Beenakker, S. Brensing, M. Kramer, A. Kulesza, E. Laenen, and I. Niessen, *Soft-gluon resummation for squark and gluino hadroproduction*. JHEP **12** (2009) 041, arXiv:0909.4418 [hep-ph].

[75] W. Beenakker, S. Brensing, M. Kramer, A. Kulesza, E. Laenen, and I. Niessen, *Supersymmetric top and bottom squark production at hadron colliders*. JHEP **08** (2010) 098, arXiv:1006.4771 [hep-ph].

[76] W. Beenakker, S. Brensing, M. n. Kramer, A. Kulesza, E. Laenen, L. Motyka, and I. Niessen, *Squark and Gluino Hadroproduction*. Int. J. Mod. Phys. **A26** (2011) 2637–2664, arXiv:1105.1110 [hep-ph].

[77] F. Ambrogi, S. Kraml, S. Kulkarni, U. Laa, A. Lessa, and W. Waltenberger, *On the coverage of the pMSSM by simplified model results*. Eur. Phys. J. **C78** (2018) no. 3, 215, arXiv:1707.09036 [hep-ph].

[78] G. Brooijmans *et al.*, "Les Houches 2017: Physics at TeV Colliders New Physics Working Group Report," in *10th Les Houches Workshop on Physics at TeV Colliders (PhysTeV 2017) Les Houches, France, June 5-23, 2017*. 2018. arXiv:1803.10379 [hep-ph]. http://inspirehep.net/record/1664565/files/1803.10379.pdf.